Atomization and Sprays, 23 (6): 517–533 (2013)

BREAKING THE RAYLEIGH-PLATEAU INSTABILITY LIMIT USING THERMOCAVITATION WITHIN A DROPLET

J. P. Padilla-Martinez,[1] J. C. Ramirez-San-Juan,[1] N. Korneev,[1] D. Banks,[2] G. Aguilar,[2] & R. Ramos-Garcia[1,*]

[1]*Departamento de Óptica, Instituto Nacional de Astrofísica, Óptica y Electrónica, Puebla, Pue. 7200, México*

[2]*Department of Mechanical Engineering, University of California Riverside, Riverside, California, 92521 USA*

[*]Address all correspondence to R. Ramos-Garcia E-mail: rgarcia@inaoep.mx

Original Manuscript Submitted: 02/06/2013; Final Draft Received: 03/21/2013

We report on the generation of liquid columns that extend far beyond the traditional Rayleigh-Plateau instability onset. The columns are driven by the acoustic pressure wave emitted after bubble collapse. A high-speed video imaging device, which records images at a rate of up to 10^5 fps, was employed to follow their dynamics. These bubbles, commonly termed thermocavitation bubbles, are generated by focusing a midpower (275 mW) continuous wavelength laser into a highly absorbing liquid droplet. A simple model of the propagation of the pressure wavefront emitted after the bubble collapse shows that focusing the pressure wave at the liquid–air interface drives the evolution of the liquid columns. Control over the aspect ratio of the liquid column is realized by adjusting the cavitation bubble's size, beam focus position, and droplet volume.

KEY WORDS: *shockwave, cavitation, spray*

1. INTRODUCTION

Control of the geometry and stability of liquid columns associated with the bubble formation and collapse that leads to column formation is of paramount importance in many processes spanning scales from macroscopic to nanometric, such as the fabrication of breathable droplets (Baron and Willeke, 1986), crop and paint-spraying (Basaran, 2002), gasoline combustion (Goldshtein et al., 1998), water waveguide (Bertin et al., 2010), inkjet printing (Martin and Hutchings, 2008) (where monodisperse microdroplets are required to accurately control ink deposition), and others. Commonly, the liquid column and droplet production are achieved primarily by various types of spraying nozzles. Nozzles have been modified with supplemental atomization mechanisms, such as stimulation

by acoustic waves (Kurosawa et al., 1995; Lang, 1962) or by electrospray atomization (Giovannini et al., 1994), where a high voltage is applied to a piezoelectric transductor to alter the break- up length of the column in order to generate micron-size droplets of conducting liquids (Warnica et al., 1993).

These processes often encounter a fundamental limitation associated with the Rayleigh-Plateau (R-P) instability. The R-P instability limit dictates the relationship between the length L of the liquid column and its mean radius R, as $\Lambda = L/2R$. In weightless conditions, a cylindrical liquid column becomes unstable and breaks up into one or more droplets when its length L exceeds its circumference (i.e., $\Lambda > \pi$). In the presence of gravity, the rupture of the liquid columns occurs for even smaller values of Λ. Over the years, several methods have been developed to achieve aspect ratios $\Lambda > \pi$, for example, by compensating for gravity with magnetic (Mahajan et al., 1999) and electric fields (Marr-Lyon et al., 2000; Raco, 1968; Gonzalez et al., 1989; Burcham and Saville, 2000) in dielectric and conducting liquids. Optical radiation pressure (Casner and Delville, 2004; Schroll et al., 2008) was also demonstrated to form liquid bridges; however, these bridges were created under very special conditions. The R-P instability limit may also be exceeded by using acoustic pressure waves (Marr-Lyon et al., 2001; Bertin et al., 2010; Tan et al., 2009) that propagate along a solid surface to concentrate its mechanical energy into a droplet set atop that surface (Tan et al., 2009). Despite much effort, the largest value reported so far for Λ is $\sim$14 (Schroll et al., 2008).

On the other hand, optical thermocavitation within a water droplet provides an alternative technique to produce liquid columns with delayed instability onset on demand. Until now, the principal mechanism for generation of cavitation bubbles within droplets has been the use of short-pulsed lasers (Carls and Brock, 1991; Zheng et al., 1991; Robert et al., 2007; Heijnen et al., 2009; Eickmans et al., 1987; Hsieh et al., 1987), where bubbles are generated by liquid optical breakdown when the laser beam is focused into a small spot. Thoroddsen et al. (2009) used a pulsed Nd:YAG laser with pulse duration of 7 ns and maximum fluency of $\sim$42 J/cm^2 per pulse. Another method of inducing cavitation within large droplets was recently studied by Obreschkow et al. (2006). In these millimeter-sized drops (8–13 mm), cavitation was generated through a spark discharge between two thin electrodes (8–1000 mJ discharge energy) while the droplet was suspended in a microgravity environment. The electrically induced cavitation produces spherical bubbles and revealed two counterpropagating liquid jets inside the droplet that disrupt the droplet's surface, producing splash. However, these methods tend to be very complex and expensive.

The present paper reports observations and a theoretical model of the evolution of thermocavitation bubbles (Ramirez-San-Juan et al., 2010, 2011; Korneev et al., 2011; Padilla-Martinez et al., 2011) formed inside a highly absorbing liquid droplet using a midpower (275 mW) continuous wavelength (CW) laser. The acoustic pressure wave (APW) produced immediately after bubble collapse creates stable liquid columns whose length exceeds its circumference ($L > 2\pi R$), beyond the traditional onset of R-P

instability. The aspect ratio of the liquid column is controlled by the laser power, position of the lens focal point, and droplet volume. This approach is simpler and less expensive than other mechanisms of liquid column generation that use magnetic or electric fields, optical radiation pressure arising from total internal reflection of the laser light inside the column, or ultrasound. Furthermore, under adequate conditions, the liquid column breaks up into secondary droplets, depending on the original droplet's volume, suggesting the potential design of an alternative droplet generator, which is simpler and cheaper than traditional on-demand droplet generators.

2. EXPERIMENT AND RESULTS

A droplet of a saturated solution of copper nitrate ($CuNO_4$) dissolved in water was used as a thermocavitation media. The absorption coefficient of the solution at the operating wavelength (λ = 975 nm) was α = 135 cm^{-1} (Ramirez–San-Juan et al., 2010). The density of the solution is approximately twice that of water ($\rho_{sol} \approx 2\rho_{wat}$), and the viscosity μ_{sol} was measured using a viscometer (Cannon-Fesnke) obtaining a value $\mu_{sol} \sim 5\mu_{water}$. The superficial tension was measured using a capillary tube (Fox et al., 2004). The rise height and capillary angle were determined through a high-quality photograph, and using the density of the solution, the superficial tension was calculated as $\sigma \sim 0.088$ N/m, which is similar to the superficial tension of water ($\sigma_{water} \sim 0.072$ N/m).

A droplet of the solution (2, 5, 10, and 20 μL volume) was confined by a thin ring-shaped plastic sticker, with an inner diameter of 5 mm and $\sim$100 μm depth, resting on an untreated glass microscope slide (1 mm thickness). Since the droplet's volume is larger than the enclosing pool's volume, the droplet takes a hemispherical shape raised above the sticker (see inset of Fig. 1). The laser beam (λ = 975 nm) was collimated and focused with a microscope objective (f = 8 mm), sitting under the microscope slide. The laser beam is strongly absorbed by the solution near the interface (glass–liquid), producing a superheated region that around 300°C undergoes an explosive phase transition (Kafalas and Ferdinand, 1973; Skripov and Pavlov, 1970; Yavas et al., 1993) and consequently, the formation of an expanding vapor bubble (Fig. 1). This temperature value is close to the prediction of classic nucleation theory for homogeneous nucleation and later confirmed by several experimental techniques (Caupin and Herbert, 2006). The vapor bubbles produced by this method are commonly termed thermocavitation bubbles. Further details concerning thermocavitation and its dynamics can be found in the literature (Rastopov and Sukhodolsky, 1992; Ramirez–San-Juan et al., 2010). The objective can be displaced vertically to change the focal position inside the droplet and thus change the beam intensity at the interface. This is to control the volume of superheated liquid available for evaporation. In order to observe the position of the laser beam focus on the microscope slide inner surface, a dichroic mirror was used to redirect the portion of the

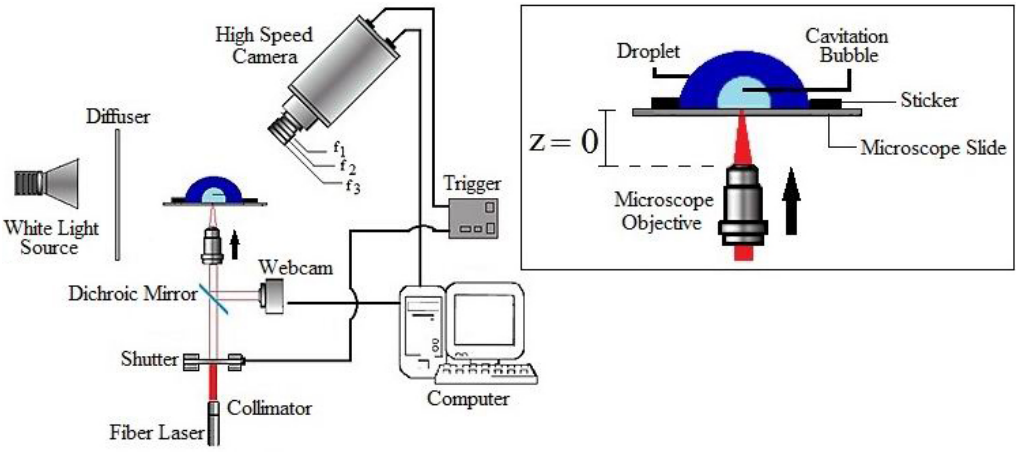

FIG. 1: Experimental setup for the analysis of liquid jets produced by thermocavitation within a droplet of $CuNO_4$. The camera was used with three lenses (f_1, f_2, and f_3) to magnify the field of view.

laser light reflected by the glass surface to a webcam. When the focus is at the interface, the spot is the smallest and it is identified as the reference level $z = 0$ (see inset of Fig. 1).

For these experiments, the laser power was fixed to 275 mW (the maximum power available for our laser system) and the bubble radius was controlled by displacing the beam focus from the interface as shown in the inset of Fig. 1. It was found that placing the laser's focus at $z = 400$ μm above the glass–liquid interface led to the largest cavitation bubbles of ∼1 mm maximum radii. In order to record the formation and evolution of the bubble inside the droplet, it was illuminated with a white light source almost perpendicular to the laser beam direction with the diffuser before the droplet. The droplet was imaged on a high-speed video camera (Phantom V7.1), which records images at a rate of up to 10^5 fps. The CW laser beam was blocked by a shutter, and when it opened (∼2 s), triggered the high-speed camera to initiate recording.

3. EXPERIMENTAL RESULTS

Figure 2 shows the formation and evolution of a single cavitation bubble within a 5 μL volume droplet. The laser light is strongly absorbed by the solution near the interface (glass–liquid) and ∼82 ms after the laser was turned on, the superheated volume produces an expanding vapor bubble (Fig. 2a). It is important to mention that the vapor bubble is attached to the glass surface at all times, taking a hemispherical shape regardless of the power and location of the laser focal point, in contrast to pulsed-laser cavitation. In pulsed-laser cavitation the bubble is created wherever the focal point is and its shape depends on the distance from the solid–liquid boundary to the center of

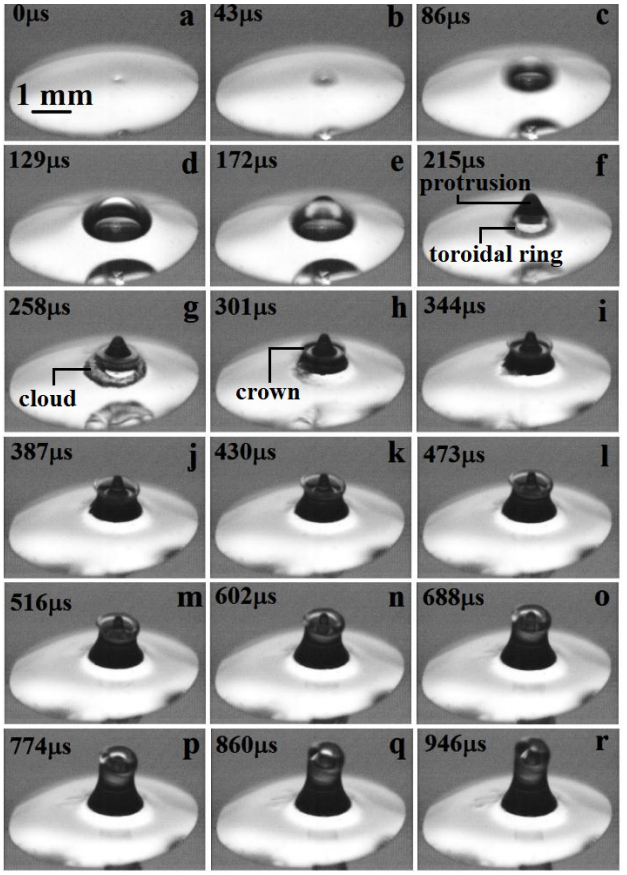

FIG. 2: Temporal evolution of a vapor bubble created inside a small droplet and the subsequent liquid column formation: (a–c) bubble formation, (d) maximum bubble expansion, (e–g) bubble collapsing, (h–l) protrusion-crown formation, and (m–r) liquid column growth from the droplet.

the bubble (Phillip and Lauterborn, 1998; Carls and Brock, 1991; Zheng et al., 1991; Robert et al., 2007; Heijnen et al., 2009; Thoroddsen et al., 2009; Eickmans et al., 1987; Hsieh et al., 1987). The bubble takes a hemispherical shape. The laser-induced bubble grows until it reaches its maximum radius ($R_{max} \sim 1$ mm) ~ 129 μs after bubble formation (Fig. 2d), causing a protrusion at the top of the droplet. When the bubble begins to collapse, the protrusion appears to stop growing (Figs. 2e–2f) but retains its shape because its dynamics is much slower than the bubble's collapse. At the final stage of collapse, the bubble takes a toroidal ring shape (although not visible in Fig. 2), because the pressure is higher near the pole of the bubble, producing a convex curvature over the bubble surface (Shima and Nakajima, 1977). The toroidal ring is unstable and collapses in several smaller bubbles, as was shown by Phillip (1998), forming a cloud of smaller

bubbles around the ring (Fig. 2g). The emission of the APW at the collapse of the bubble produces a crown around the base of the protrusion. The ejected protrusion-and-crown outside the droplet continues to enlarge and merge into a single column (Figs. 2i–2r). For illustration purposes, images are shown until ∼1 ms but the liquid column (shown in Fig. 2r) continues growing up to ∼5 ms, where it reaches a height of ∼10 mm and a diameter of 0.5 mm, giving $\Lambda = 20$, i.e., almost 6 times larger than the R-P instability limit for weightless conditions.

The width and height of the liquid column can be influenced by the laser parameters and the droplet's volume. The laser power and beam focus position determine the bubble size and consequently, the APW amplitude driving the column's formation (Korneev et al., 2011; Padilla-Martinez et al., 2011) and force exerted on the interface, while the droplet volume determines the width and height of the liquid column. In order to determine the effect of the APW, the laser focus position was varied from $z = 0$ to $z = 400$ μm in intervals of 100 μm, inside a droplet of 20 μL volume. Figure 3 shows that for $z \leq 300$ μm the droplet's surface was perturbed but no liquid column is formed. A liquid column was obtained only when the cavitation bubble was the largest possible (∼1 mm radius), which happened at $z = 400$ μm. After setting the power and laser focus position in the experimental setup, the only way to control the length and width of the liquid column was by changing the droplet volume.

Figure 4 shows high-speed photographs of the liquid column formed for three different droplet volumes (20, 10, and 5 μL volume). The first picture of each row is the onset of a liquid column (protrusion) following bubble collapse. For a droplet of 20 μL volume (Fig. 4a), the liquid column is ejected with a velocity ∼1 m/s. As the jet rises, it

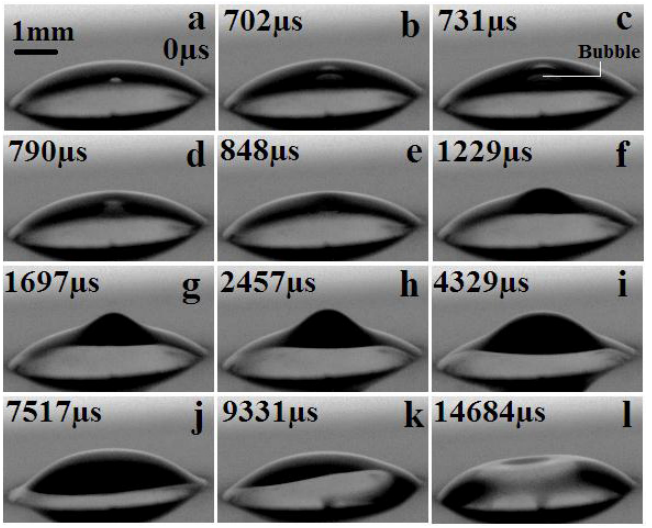

FIG. 3: (a–b) Vapor bubble formation at $z = 300$ μm, (c) maximum bubble expansion, (d–e) bubble collapsing and APW emission, and (f–l) droplet perturbation due the APW.

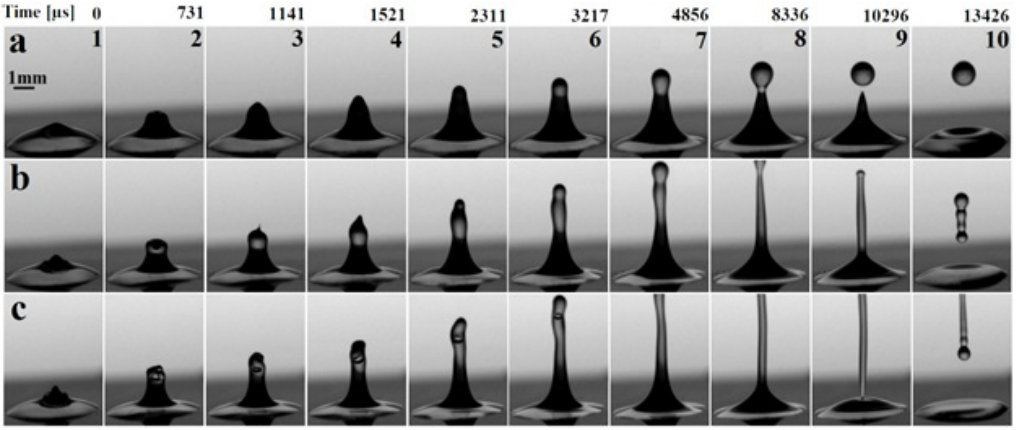

FIG. 4: Liquid column formation by thermocavitation. The vertical columns show pictures at the same time but different initial droplet volumes: (a) 20, (b) 10, and (c) 5 μL.

narrows and ultimately breaks apart as R-P instability grows (Fig. 4a, 8). Eventually, surface tension causes the jet to pinch off and form a spherical secondary droplet (Fig. 4a, 10). The secondary droplet falls back into the bulk solution and its dynamics is similar to that produced by a droplet impinging in a water pool (Yarin, 2006; Manzello and Yang, 2002).

In Fig. 4, the amplitude of the APW is the same in all cases, but as the droplet volume decreases, the APW becomes more concentrated and is able to drive the liquid column higher (Figs. 4b and 4c). The initial liquid column velocities are ∼1.3 m/s for 10 μL volume and ∼1.7 m/s for 5 μL volume. These velocities are much smaller than those obtained with cavitation within a droplet using short-pulsed lasers, where velocities in the range of 100–250 m/s for microjets of 5–50 μm diameter (Thoroddsen et al., 2009) were reported. However, in those studies, no measurements of the Λ parameter were reported. From Fig. 4, the onset of the R-P instability for the 20 μL volume occurs for $\Lambda = 2.98$ (Fig. 4a, 6) and $\Lambda = 8.3$ for the 10 μL volume (Fig. 4b, 7). For the last case (5 μL volume), the liquid column extends beyond the limits of the field of view (Fig. 4c, 7). The increase in length between the first two cases, doubles (see Figs. 4a, 6 and 4c, 7) and assuming that this trend is valid for the 5 μL case (Fig. 4c, 8), then $\Lambda = 20$, i.e., the R-P limit is extended at least 40% beyond previous reports (Schroll et al., 2008).

Finally, when the pool was filled with ∼2 μL volume it was possible to produce a liquid column even for $z = 0$. For that reason, the laser focus position was varied from $z = 0$ to $z = 400$ μm in 100 μm intervals (Fig. 5). As the laser focus moves beyond the liquid surface, the bubble size increases. It may seem contradictory that cavitation bubbles are created when the laser focus is outside the solution ($z \geq 100$ μm,), but remember that the attenuation distance is ∼75 μm (<pool depth = 100 μm), so the effect of increasing z is to increase the volume available for explosive phase transition.

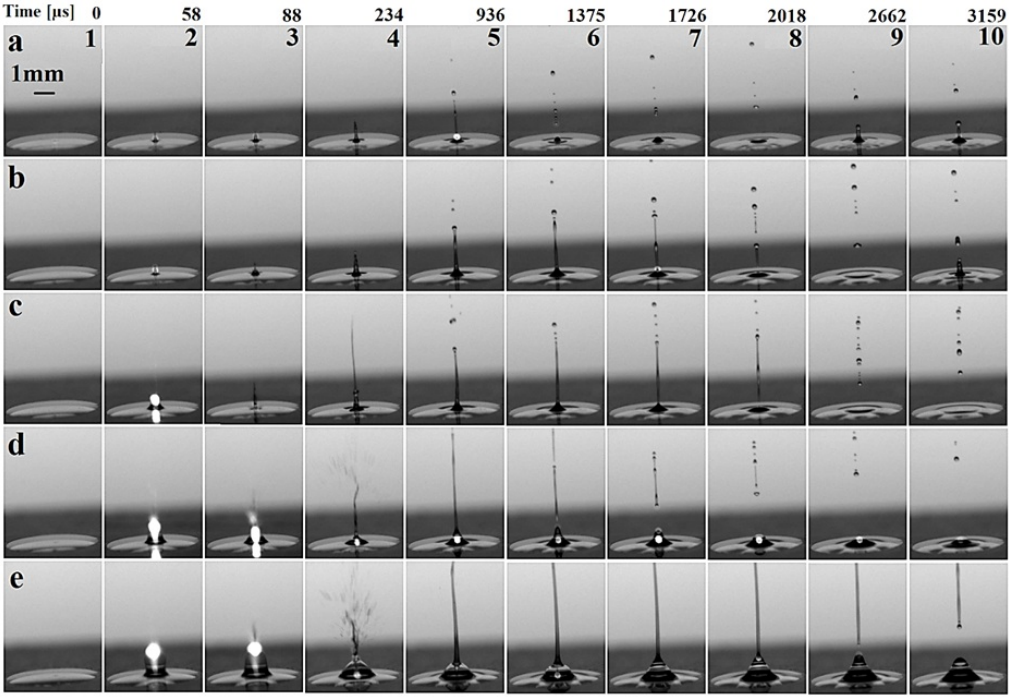

FIG. 5: Liquid column formed by thermocavitation on a solution thin film (100 μm thickness). The vertical column shows pictures at the same time but different laser focus positions: (a) $z = 0$, (b) $z = 100$, (c) $z = 200$, (d) $z = 300$, and (e) $z = 400$ μm above the glass–liquid interface.

For $z = 0$ until 200 μm, a definitive trend is evident: the bubble size, APW amplitude, the velocity (3.7, 4.3, 22.2 m/s, respectively), and the height of the liquid column are increasing with z, but the radius of the column is decreasing (Figs. 5a–5c), obtaining aspect ratios of $\Lambda \sim 10$, 15, and 42, respectively. However, for $z = 300$ μm (Fig. 5d) the surface solution is broken due to the large kinetic energy imparted by the APW producing a splash and smaller droplets or spray. The same dynamics have been observed in cavitation within droplets induced by short-pulsed lasers (Thoroddsen et al., 2009; Apitz, 2005; Kim et al., 1998). After this breakup, the liquid closes up due to surface tension, leading to a tall and narrow liquid column reaching an aspect ratio of $\Lambda \sim 46$. In the case of $z = 400$ μm, a fine spray is obtained earlier and also a liquid column can be formed (Fig. 5e). This is an interesting phenomenon that could be used for the generation of pulsed transient sprays. In order to study in more detail the column formation after the liquid breakup, the same experiment with a sample rate of 50,000 fps was repeated. Figure 6 shows a closeup of the formation and evolution of a fine spray which is expelled from the liquid after bubble collapse. The vertical walls of the spray are expelled at speeds around 26 m/s, forming a conical crown (Figs. 6a–6g). The walls of the liquid

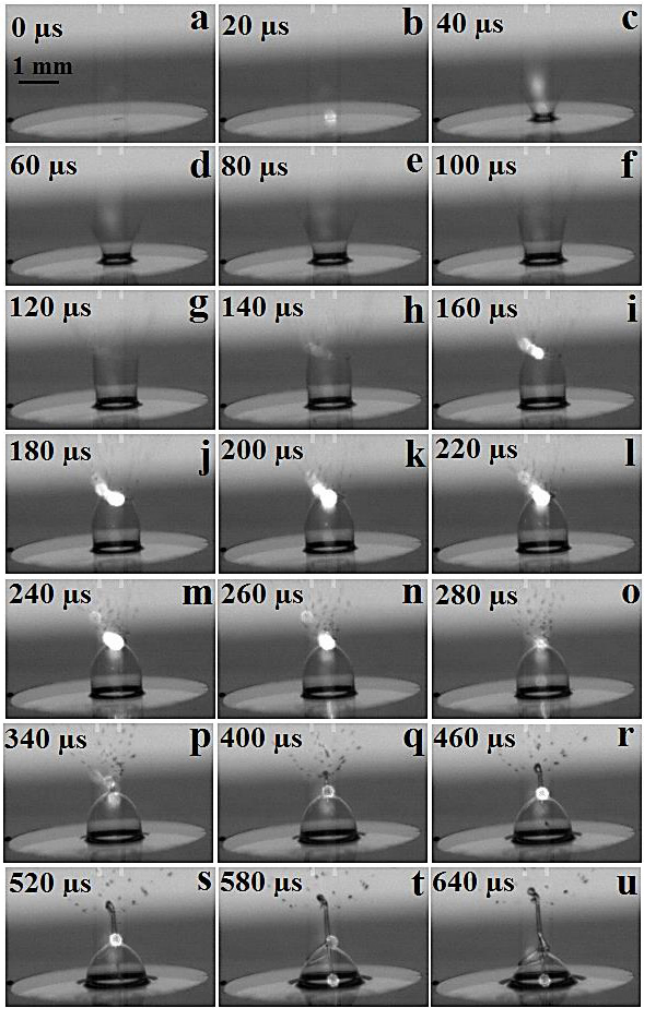

FIG. 6: The formation of fine spray by thermocavitation: (a–g) generation of vertical walls (laser-induced crown), (i–p) bubble formation by the suction of the vertical walls, and (q–r) liquid column formation on the upper part of the bubble. The images were taken at z = 400 μm.

cone close up due to the surface tension, trapping an air bubble in the center of the pool (Figs. 6h–6k). In the work of Thoroddsen et al. (2009), the air bubble trapped in the droplet was attributed to suction due to lower pressure of the plasma; however, in our experiments no observable plasma is produced. Because the liquid continues its upward displacement over the walls of the bubble, due to their high momentum, they symmetrically collide on the apex producing two counterpropagating liquid columns, one directed toward the air bubble and the other moving upward (Figs. 6q–6u). This

narrow column is found to reach velocities of ∼12.5 m/s, whose height could not be determined because it grows beyond the field of view (Fig. 5e, 6). The aspect ratio in this case is at least >46.

4. DISCUSSION

As mentioned before, the relative importance of inertial force and surface tension can be controlled by changing the droplet volume and amplitude of the APW. The relative importance of viscosity and surface tension in the behavior of a liquid column is expressed through the Ohnesorge number [Eq. (1)], which prescribes the relative importance of viscous stresses and curvature pressures, and Weber number [Eq. (2)], which represents the relative importance of the fluid's inertia compared to its superficial tension,

$$\mathrm{Oh} = \frac{\mu}{\sqrt{\rho_{sol}\sigma R}}, \tag{1}$$

$$\mathrm{We} = \frac{\rho_{sol} U^2 R}{\sigma}, \tag{2}$$

where μ is the viscosity, ρ_{sol} is the density, σ the superficial tension, and R the radius of the column (measured in the middle part of column) and U its initial velocity. As the Ohnesorge number is much less than 1 for the cases of 5, 10, and 20 μL volume (Oh = 0.009, 0.008, and 0.006, respectively), then liquid viscosity has a minimal effect on the liquid column dynamics. On the other hand, the Weber number being much larger than 1 indicates that inertial force dominates the droplet behavior (We $>$ 10 for the three volumes). Figure 7a shows the temporal evolution of the liquid column length for four different volumes at z = 400 μm. Figure 8a shows also the temporal evolution for ∼2 μL of solution volume but different laser focus positions. In both figures it can be observed that the column's length is larger as droplet's volume decreases or when the laser focus increases. The slope of the dashed lines indicates the initial velocity of the columns.

Figures 4, 5, 7b, and 8b indicate that two regimes of liquid column formation can be distinguished: (i) cavitation and (ii) splash dominated. In the second case, rupture of the liquid occurs and has been studied extensively (Thoroddsen et al., 2009; Apitz, 2005; Kim et al., 1998), so this regime will not be discussed here. In the first case, however, the liquid column formation is due to the concentration of mechanical energy (Tan et al., 2009) at the solution–air interface as described below. Note that the R-P limit in both cavitation and splash-dominated cases is larger than previous reports.

4.1 Breaking the R-P Limit: Cavitation

The APW produced at the moment of the collapse propagates through the droplet with a velocity of ∼1800 m/s (with frequency ω_{APW} = 480 kHz and λ_{APW} = 3.75 mm), taking just ∼0.5 μs to reach the droplet's surface from the implosion point. The velocity of the

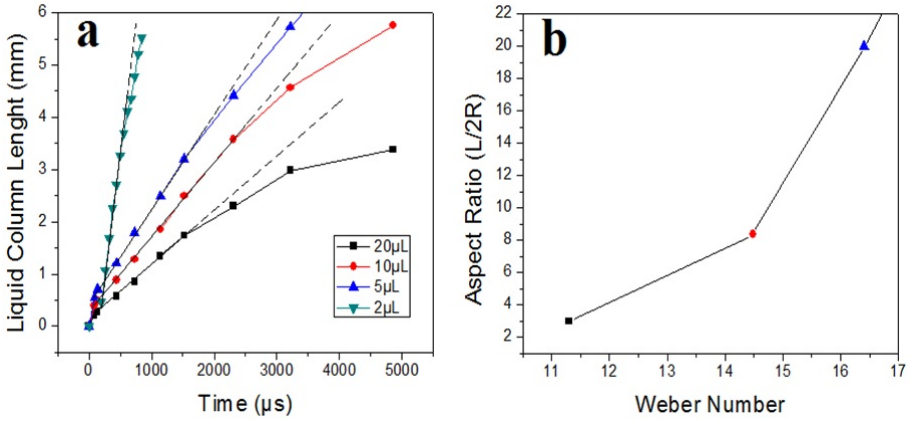

FIG. 7: (a) Liquid column length as a function of time at four different volumes and z = 400 μm. The dashed black lines indicate a fit to the data and the slope represents the initial velocity of the ejected column. (b) Aspect ratio versus Weber number. Continuous lines are connecting lines.

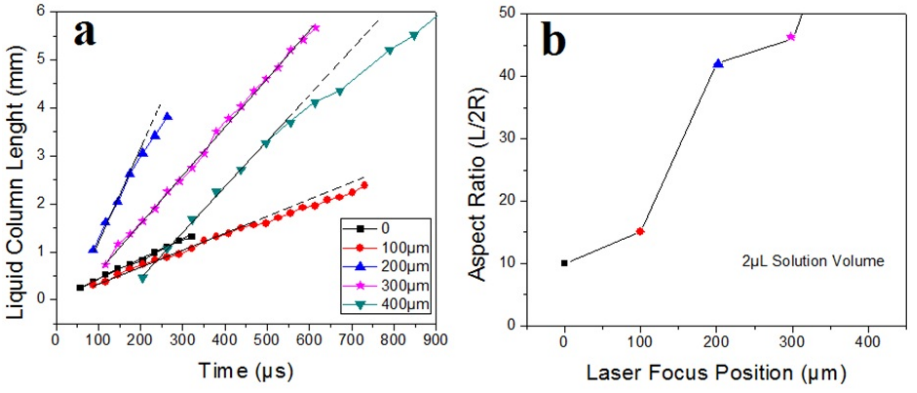

FIG. 8: (a) Liquid column length as a function of time at different z values for the 2 μL solution. (b) Aspect ratio versus the laser focus position. Continuous lines are guides to the eye only.

APW was measured by taking the time interval between two hydrophones separated a fix distance. Typical values of the magnitude of the APW lies in the range of ∼1 MPa for a vapor bubble of ∼300 μm radius (Ramirez–San-Juan et al., 2010). Due to impedance mismatch (I_{air} = 413.3 and $I_{solution}$ = 3.6 × 10^6 Ns/m^3 at 20°C) between the solution and air, the pressure wave will be reflected. The fraction of the incident wave that is reflected is given by $R = [(I_{air} - I_{solution}) / (I_{air} + I_{solution})]^2$, obtaining a value of $R \sim 0.999$. This shows that the liquid–air interface acts as a perfect mirror, reflecting the pressure wave back into the liquid and generating multiple reflections inside the droplet

until its amplitude attenuates due to losses (Ramirez–San-Juan et al., 2010). Reflection of the APW on the liquid–air interface changes the moment of the wave and therefore a force is exerted on each interface. The distribution of wave momentum transmitted to the surface at first reflection is rather smooth. However, for the second reflection and for appropriate droplet parameters, the formation of an acoustic wavefront singularity (caustic) inside a droplet is possible, i.e., the APW will be focused at the liquid-air interface deforming the liquid surface producing a crown around the base of the protrusion (Figs. 2g–2h). The crown's speed emerges out at velocities of about 1.7 m/s, forming a characteristic protrusion-and-crown shape, similar to that generated by droplet impact on liquid pools (Yarin, 2006; Manzello and Yang, 2002).

In order to prove this claim, a computer simulation of the wavefront shape after propagation, in the approximation of a small wavelength (i.e., using ray tracing), was made. The droplet with radius r was modeled as a semispherical cap above the plane $y = a$ with the source at the point $x = z = 0$, $y = a$ (Fig. 9). The a parameter determines the volume of the droplet and the proximity of the source to the liquid–air interface. It was also assumed that the shape of the droplet's surface does not change appreciably after the reflection, otherwise the problem is too complicated to simulate. In the following, we consider the plane $Z = 0$ only, which is possible because of the cylindrical symmetry of the problem. A ray emitted from the origin makes an angle θ with the X-axis and its subsequent impact points at the interfaces are X_1, X_2, and so on. For our purposes only the point X_2, where the wavefront hits the liquid–air interface, will be relevant to our analysis. The inset picture in Fig. 9 shows a pair of rays representing the wavefronts inside the real droplet. In Fig. 10 some characteristic wavefronts for $a = 0.3$, which

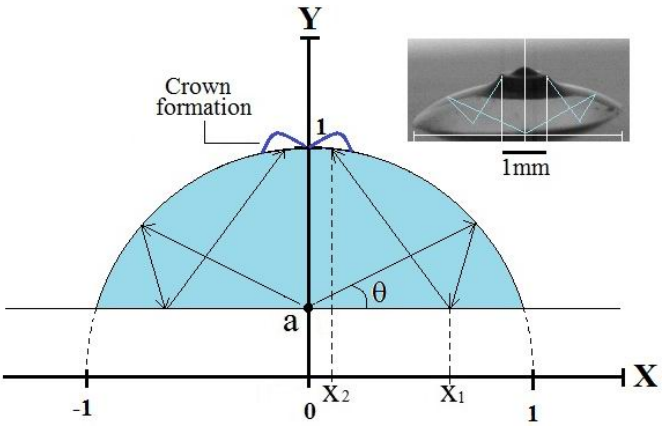

FIG. 9: The droplet geometry and ray tracing. The droplet is limited by a spherical cap with a radius $r = 1$ and by a plane $Y = a$. The pressure wave is emitted at the origin. The acoustic ray is characterized by an initial angle θ. The X coordinates of consequent arrivals of the ray at the spherical surface are X_1, X_2, and so on. The inset shows the real drop and two rays are drawn for illustration purposes. See text for details.

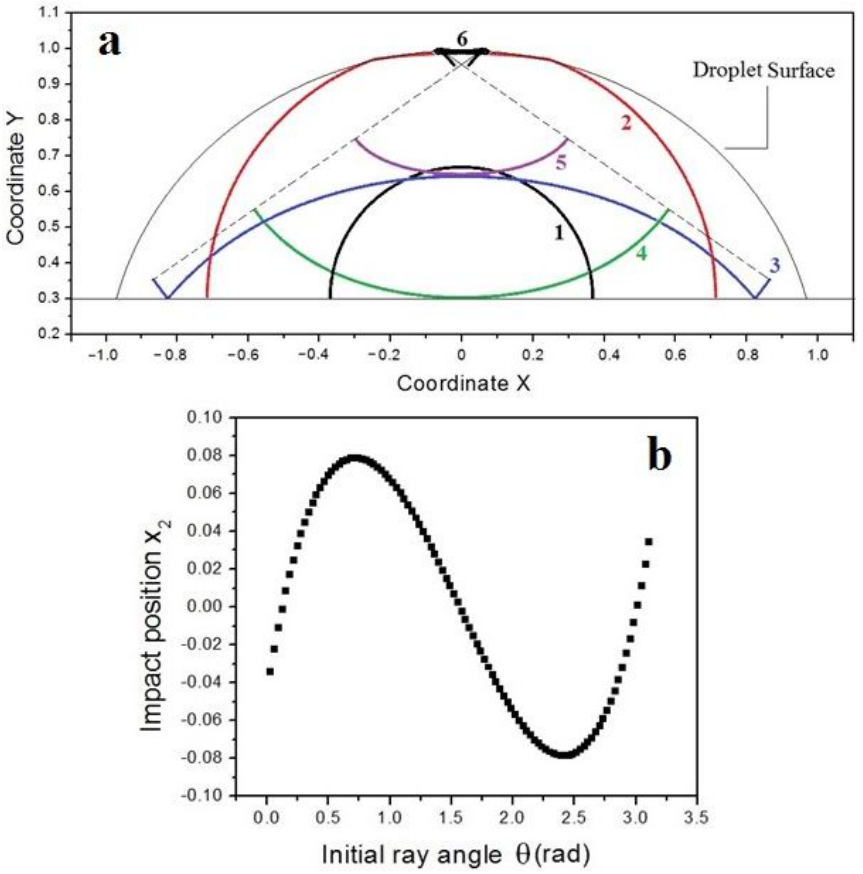

FIG. 10: (a) Consequent waveform shapes. First, the wave is spherical (1). The spherical droplet surface acts as a focusing mirror with a high degree of aberration (2–5). After reflection on the water–glass interface, the wave is strongly concentrated close to the droplet free surface (6). (b) The dependence of the X_2 coordinates on the second arrival on the initial ray angle (see Fig. 9). The maximal X_2 value ($\sim$0.079) corresponds to the wavefront singularity position.

correspond to the case of larger droplet volume, are depicted. Label 1 represents a wavefront traveling toward the droplet surface. The wavefront (2) just arrived to the droplet surface and then it is totally reflected (3) and reflected back again at the glass–liquid interface (4). The wavefront after this reflection is being focused (5), and finally, the wave becomes highly focused (6) at the liquid–air interface. In each reflection momentum is transferred and therefore a force is exerted on the interface which eventually will deform it, as graphically indicated in the inset of Fig. 9.

Note from Fig. 10 that only a fraction of a wavefront is being focused, suggesting that this fraction depends on the initial ray angle. The momentum density is defined as

dP/dA, where P is the momentum transferred to the liquid–air interface and $dA(= dzdX)$ is the area element on the droplet surface. Note dX around the maximal X_2 tends to zero, so the maximum value in X-coordinate produces a singularity in the transmitted momentum density and therefore a singularity in pressure. This phenomenon is similar to a rainbow formation mechanism. Figure 10b shows that for a = 0.3, there are two symmetric positions from the origin where the momentum density is maximal ($X_2 = \pm 0.079$) for rays emitted at angle of $\theta = \pm 0.75$ rad. Thus one can expect the formation of small annular regions where the acoustic wave energy, and consequently, the transmitted momentum, is much higher than the average. The exact position of these regions sensitively depends on the droplet shape at the moment of bubble collapse. For a = 0.7 the caustic is formed upon the third arrival to the surface, contrasted with the second for a = 0.3; however, the general behavior is similar. The inset of Fig. 9 illustrates this situation.

Thus our simple simulations describe qualitatively well the formation of liquid columns. The focusing of the APW at the liquid–air interface at two symmetric positions around the apex of the droplet deforms the liquid surface, producing a crown around the base of the protrusion as observed in the experiment (Figs. 2g and 2h). Although the simulations do to take into account the initial protrusion on the droplet, one can see from Fig. 10 that most of the momentum is not transferred from the central part of the wavefront but from rays emitted at certain angles. Subsequent reflections from the deformed droplet may contribute to its continuous growth, but we believe that transfer of momentum at the first reflection at the liquid–air interface is the main driving force of the growth of the liquid column and breaking of the R-P limit.

5. CONCLUSIONS

We showed a novel mechanism of continuous-wave optical cavitation to generate vapor bubbles within a droplet and the subsequent generation of liquid columns that greatly surpass the R-P limit (i.e., do not break into droplets until its length is $\sim$14 times larger than its circumference). We used a CW laser focused in a highly absorbent solution, featuring an experimental setup that is less complex than pulsed-laser setups to achieve similar results. Furthermore, the mechanism of bubble formation is demonstrated to be different than the mechanism of creation using pulsed lasers or electrical discharge inside the droplet; however, the ejected liquid column from the droplet is very similar but with a lower jet velocity (3–12 m/s) than the velocities reported with pulsed lasers. A simple model based in ray tracing shows that APW drives the dynamics of column formation. One potential application of this phenomenon is found in the liquid column generated after the bubble collapse, which could be used like an acoustic waveguide, as was shown by Bertin et al. (2010).

ACKNOWLEDGMENTS

The authors appreciate the financial support from CONACyT through project CB-2010-153463. The authors acknowledge financial support from CONACyT-Mexico and an Omnibus Academic Senate Research Grant, UCR. Also a special thanks to Josue Lopez for laboratory assistance.

REFERENCES

Apitz, I. and Vogel, A., Material ejection in nanosecond Er:YAG laser ablation of water, liver, and skin, *Appl. Phys. A.*, vol. **81**, no. 2, pp. 329–338, 2005.

Baron, P. A. and Willeke, K., Respirable droplets from whirlpools: Measurements of size distribution and estimation of disease potential, *Environ. Res.*, vol. **39**, no. 1, pp. 8–18, 1986.

Basaran, O. A., Small-scale free surface flows with breakup: Droplet formation and emerging applications, *AIChE J.*, vol. **48**, pp. 1842–1848, 2002.

Bertin, N., Wunenburger, R., Brasselet, E., and Delville, J. P., Liquid-column sustainment driven by acoustic wave guiding, *Phys. Rev. Lett.*, vol. **105**, pp. 164–501, 2010.

Burcham, C. L. and Saville, D. A., The electrohydrodynamic stability of a liquid bridge: Microgravity experiments on a bridge suspended in a dielectric gas, *J. Fluid Mech.*, vol. **405**, pp. 37–56, 2000.

Carls, J. C. and Brock, J. R., Laser-induced breakout and detonation waves in droplets, II. Model, *J. Opt. Am. B*, vol. **8**, pp. 329–336, 1991.

Casner, A. and Delville, J. P., Lasers-sustained liquid bridges, *Europhys. Lett.*, vol. **65**, no. 3, pp. 337–343, 2004.

Caupin, F. and Herbert, E., Cavitation in water: A review, *C. R. Phys.*, vol. **7**, no. 9, pp. 1000–1017, 2006.

Eickmans, J. H., Hsieh, W. S., and Chang, R. K., Laser-induced explosion of H_2O droplets spatially resolved spectra, *Opt. Lett.*, vol. **12**, pp. 22–24, 1987.

Fox, R., McDonald, A., and Pritchard, P., *Introduction to Fluid Mechanics*, 6th ed., p. 33, John Wiley and Sons, New York, 2004.

Giovannini, A., Guyomar, D., Gschwind, M., and Fonzes, G., Evaluation and design of new piezoelectrical droplets generator, *Proc.-IEEE Ultrason. Symp.*, vol. **1**, pp. 611–614, 1994.

Goldshtein, V., Goldfard, I., Schrieber, I., and Zinovier, A., Oscillations in a combustible gas bubble, *Combust. Theory Modell.*, vol. **2**, pp. 1–17, 1998.

Gonzalez, H., McCluskey, F. M. J., Castellanos, A., and Barrero, A., Stabilization of dielectric liquid bridges by electric fields in the absence of gravity, *J. Fluid Mech.*, vol. **206**, pp. 545–561, 1989.

Heijnen, L., Quinto-Su, P., Zhao, X., and Ohl, C. D., Cavitation within a droplet, *Phys. Fluids*, vol. **21**, p. 091102, 2009.

Hsieh, W. F., Zheng, J. B., Wood, C. F., Chu, B. T., and Chang, R. K., Propagation velocity of laser-induced plasma inside and outside a transparent droplet, *Opt. Lett.*, vol. **12**, pp. 576–578, 1987.

Kafalas, P. and Ferdinand, Jr., A. P., Fog droplet vaporization and fragmentation by a 10.6-μm laser pulse, *Appl. Opt.*, vol. **12**, pp. 29–33, 1973.

Kim, D., Ye, M., and Grigoropoulos, C. P., Pulsed laser-induced ablation of absorbing liquids and acoustic-transient generation, *Appl. Phys. A*, vol. **67**, pp. 169–181, 1998.

Korneev, N., Rodriguez-Montero, P., Ramos-García, R., Ramirez-San-Juan, J. C., and Padilla-Martinez, J. P., Ultrasound induced by cw laser cavitation bubbles, *J. Phys: Conf. Ser.*, vol. **278**, pp. 12–29, 2011.

Kurosawa, M., Watanabe, T., Futami, A., and Higuchi, T., Surface acoustic wave atomizer, *Sens. Actuators, A*, vol. **50**, pp. 69–74, 1995.

Lang, R. J., Ultrasonic atomization of liquid, *J. Acoust. Soc. Am.*, vol. **34**, pp. 6–8, 1962.

Mahajan, M. P., Zhang, S., Tsige, M., Taylor, P. L., and Rosenblatt, C., Stability of magnetically levitated liquid bridges of arbitrary volume subjected to axial and lateral gravity, *J. Colloid Interface Sci.*, vol. **213**, p. 592, 1999.

Manzello, S. L. and Yang, J. C., An experimental study of a water droplet impinging on a liquid surface, *Exp. Fluids*, vol. **32**, pp. 580–589, 2002.

Marr-Lyon, M. J., Thiessen, D. B., Blonigen, F. J., and Marston, P. L., Stabilization of electrically conducting capillary bridges using feedback control of radial electrostatic stresses and the shapes of extended bridges, *Phys. Fluids*, vol. **12**, no. 5, pp. 986–995, 2000.

Marr-Lyon, M. J., Thiessen, D. B., and Marston, P. L., Passive stabilization of capillary bridges in air with acoustic radiation pressure, *Phys. Rev. Lett.*, vol. **86**, no. 11, pp. 2293–2296, 2001.

Martin, G. D. and Hutchings, I. M., Inkjet printing-The physics of manipulating liquid jets and drops, *J. Phys.: Conf. Ser.*, vol. **105**, p. 012001, 2008.

Obreschkow, D., Kobel, P., Dorsaz, N., Bosset, A., Nicollier, C., and Farhat, M., Cavitation bubble dynamics inside liquid drops in microgravity, *Phys. Rev. Lett.*, vol. **97**, p. 094502, 2006.

Padilla-Martinez, J. P., Aguilar, G., Ramírez-San-Juan, J. C., and Ramos-García, R., Temporal evolution of thermocavitation bubbles using high speed video camera, *Proc. SPIE*, vol. **8097**, p. 8097271–6, 2011.

Phillip, A. and Lauterborn, W., Cavitation erosion by single laser-produced bubbles, *J. Fluid Mech.*, vol. **361**, pp. 75–116, 1998.

Raco, R. J., Electrically supported column of liquid, *Science*, vol. **160**, pp. 311–312, 1968.

Ramirez-San-Juan, J. C., Padilla-Martinez, J. P., Zaca-Moran, P., and Ramos-Garcia, R., Microhole drilling in thin films with cw low power lasers, *Opt. Mater. Express*, vol. **1**, no. 4, pp. 598–604, 2011.

Ramirez-San-Juan, J. C., Rodriguez-Aboytes, E., Martinez-Canton, A. E., Baldovino-Pantaleon, O., Robledo-Martinez, A., Korneev, N., and Ramos-Garcia, R., Time-resolved analysis of cavitation induced by Cw lasers in absorbing liquids, *Opt. Express*, vol. **18**, pp. 8735–8743,

2010.

Rastopov, S. F. and Sukhodolsky, A. T., Sound generation by thermocavitation induced CW-laser in solutions, *Proc. SPIE*, vol. **1440**, pp. 127–134, 1990.

Robert, E., Lettry, J., Farhat, M., Monkewitz, P. A., and Avellan, F., Cavitation bubble behavior inside a liquid jet, *Phys. Fluids*, vol. **19**, p. 067106, 2007.

Schroll, R. D., Brasselet, E., Zhang, W. W., and Delville, J. P., Bridging dielectric fluids by light: A ray optics approach, *Eur. Phys. J. E*, vol. **2**, pp. 405–409, 2008.

Shima, A. and Nakajima, K., The collapse of non-hemispherical bubble attached at solid wall, *Fluid Mech.*, vol. **80**, no. 2, pp. 369–391, 1977.

Skripov, V. P. and Pavlov, P. A., Explosive boiling of liquids and fluctuation nucleus formation, *High Temp. (USSR)*, vol. **8**, pp. 782–787, 1970.

Tan, M. K., Friend, J. R., and Yeo, L. Y., Interfacial jetting phenomena induced focused surface vibrations, *Phys. Rev. Lett.*, vol. **103**, p. 024501, 2009.

Thoroddsen, S. T., Takehara, K. T., Etoh, G., and Ohl, C. D., Spray and microjets produced by focusing a laser pulse into a hemispherical droplet, *Phys. Fluids*, vol. **21**, p. 112101, 2009.

Warnica, W. D., Van Reenen, M., Renksizbulut, M., and Strong, A. B., Charge synchronization for a piezoelectric droplet generator, *Rev. Sci. Instrum.*, vol. **64**, p. 2334, 1993.

Yarin, A. L., Droplet impact dynamics: Splashing, spreading, receding, bouncing, *Annu. Rev. Fluid Mech.*, vol. **38**, pp. 159–192, 2006.

Yavas, O., Leiderer, P., Park, H. K., Grigoropoulos, C. P., Poon, C. C., Leung, W. P., Do, N., and Tam, A. C., Optical reflectance and scattering studies of nucleation and growth of bubbles at a liquid–solid interface induced by pulsed laser heating, *Phys. Rev. Lett.*, vol. **70**, pp. 1830–1833, 1993.

Zheng, J. B., Hsieh, W. F., Chen, S., and Chang, R. K., Laser induced breakout and detonation waves in droplets, I: Experiments, *J. Opt. Am. B*, vol. **8**, pp. 319–328, 1991.